Electronic Supplementary Material (ESI) for Journal of Materials Chemistry A.
This journal is © The Royal Society of Chemistry 2023

Tuning LiF content in SEI by engineering the molecular structures of porous organic polymers for solid-state lithium metal batteries

Shi Zhou[1], Yiting Zhu[1], Haoran Hu[1], Chenghan Li[1], Jie Jiang*[1,2], Jianyu Huang*[1,3], Biao Zhang*[1,2]

Affiliations:

[1]School of Materials Science and Engineering, Xiangtan University, Xiangtan 411105, China;

[2]Key Laboratory of Low Dimensional Materials and Application Technology, Ministry of Education, Xiangtan University, Hunan, 411105, China.

[3]Clean Nano Energy Center, State Key Laboratory of Metastable Materials Science and Technology, Yanshan University, Qinhuangdao 066004, China.

*Corresponding author: E-mail: jiangjie@xtu.edu (JJ); jyhuang8@hotmail.com (JH); xiaobiao_zhang@outlook.com (BZ).

Electrochemical measurements and cell assembly

The composite solid electrolyte (CSE) were sandwiched between two inert stainless steel (SS) electrodes and assembled into coin cells (CR2025). The ionic conductivity at different temperatures (from 30 to 60 °C) was measured in an electrochemical station (CHI660E, Shanghai Chenhua) in a frequency range between 1 MHz and 0.01 Hz. The ionic conductivity of the polymer electrolyte was calculated using the following equation,

$$\sigma = \frac{l}{RS}$$

where l is the thickness of the SPE, R is the bulk resistance of the polymer, and S is the area of contact between the SPE and inert electrode.

The ion transport number of the CSE was calculated by the Bruce–Vincent–Evans equation

$$t^{+} = \frac{I_{ss}(\Delta V - I_0 R_0)}{I_{oo}(\Delta V - I_s R_s)}$$

where ΔV is the polarization voltage (ΔV= 10 mV), I_0 and I_{SS} are the initial current before polarization and the stable current after polarization, and R_0 and R_{SS} are the resistance before and after polarization, respectively.

The electrochemical stability windows of the composite electrolyte were evaluated by linear sweep voltammetry (LSV) at a scanning rate of 0.1 mV s^{-1} in the potential range of 0 to 6 V at 60 °C. Stainless steel was used as a working electrode and Li metal was used as a reference and counter electrode.

For the battery performance test, $LiFePO_4$ (LFP) ($LiNi_{0.8}Co_{0.1}Mn_{0.1}O_2$ (NCM811)), Super-P and poly(vinylidene fluoride) dissolved in NMP with a mass ratio of 8 : 1 : 1 were mixed and coated on an aluminium foil, and dried in a vacuum oven at 100 °C for 12 h. The mass load of LFP was 2 mg cm^{-2}. Coin cells (CR2025) were used to conduct the charge–discharge cycle test in a LAND CT2003A testing system (Wuhan LAND Electronics Co.). The test voltage range of LFP cells was between 2.5–4.1 V, and The test voltage range of NCM811 cells was between 2.8–4.3 V.

Cyclic voltammetry (CV) measurements for the Li//CSE//SS cells with different electrolyte were tested with a voltage range of 0-2.5 V and a scanning rate of 0.1 mV S^{-1}.

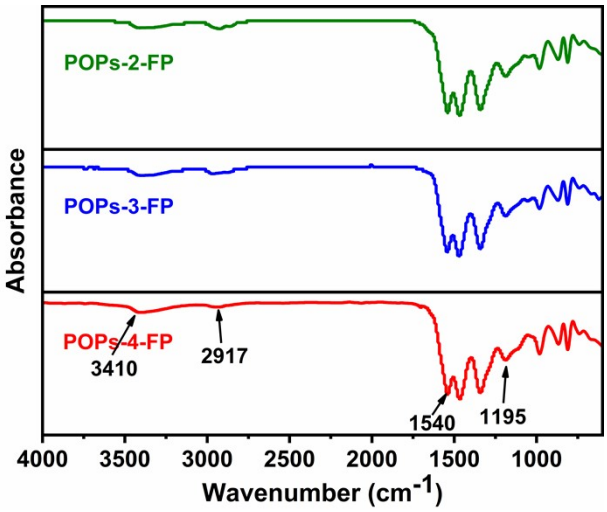

Figure S1. FTIR spectra of the POPs-X-FP

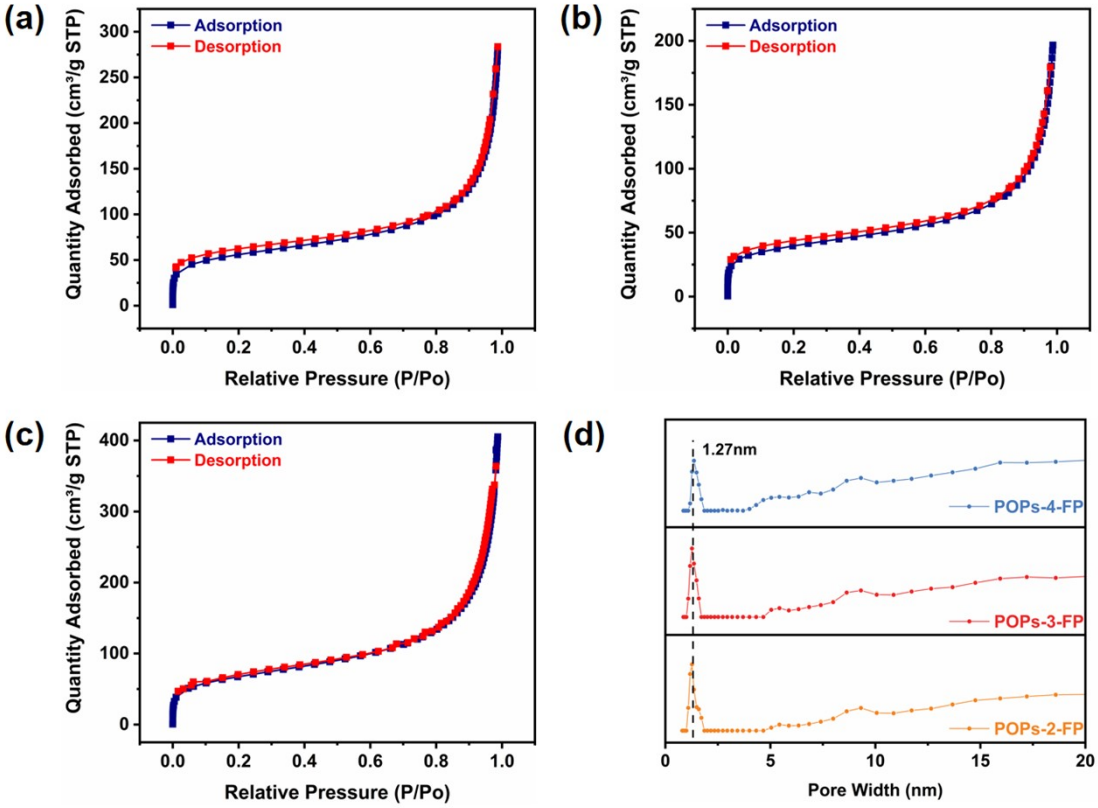

Figure S2. Adsorption (fifilled) and desorption (empty) isotherms of nitrogen (a) POPs-2-FP (b) POPs-3-FP (c) POPs-4-FP (d) Pore size distribution curves for the POPs-X-FP calculated by NLDFT.

Table S1. The porosity parameters of the POPs-X-FP

	S_{BET} (m^2/g)	V (cm^3/g)
POPs-2-FP	199	0.42
POPs-3-FP	141	0.29
POPs-4-FP	241	0.62

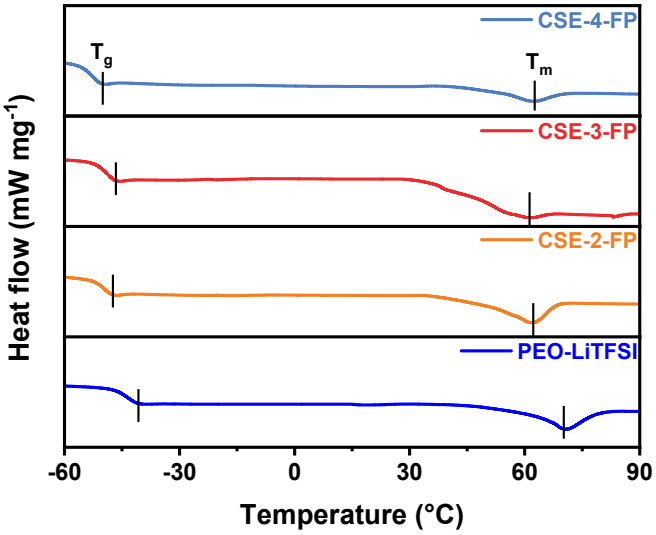

Figure S3. DSC Curves of the CSE-X-FP and PEO+LiTFSI

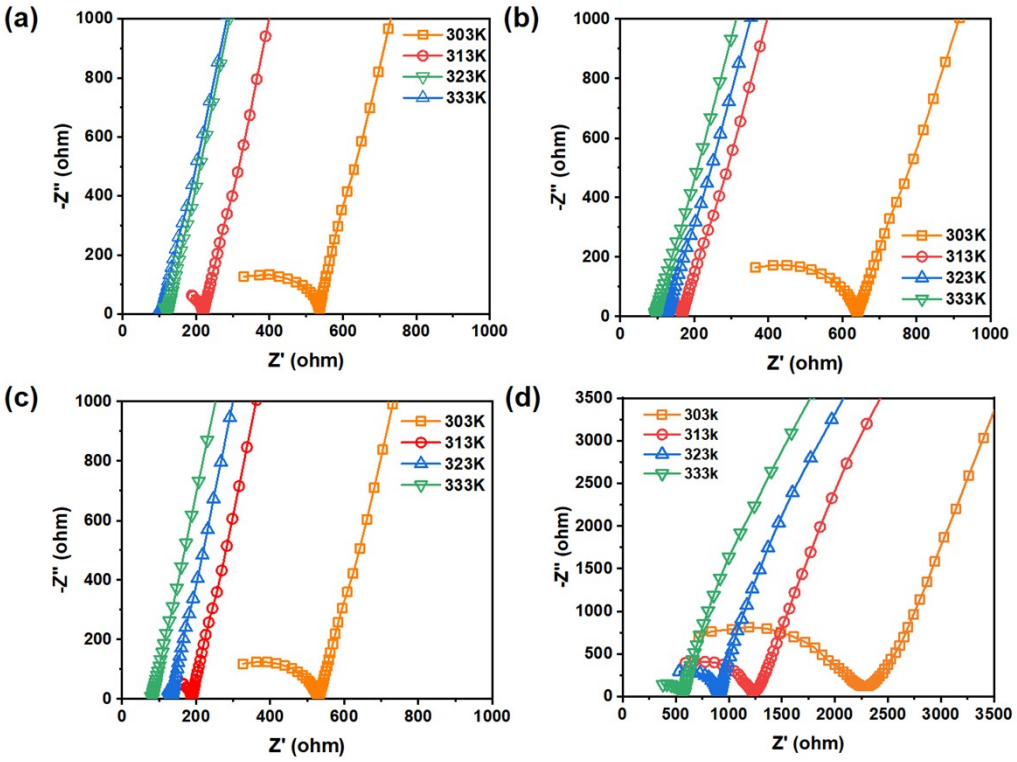

Figure S4. Impedance spectra at different temperatures. (a) CSE-2-FP. (b) CSE-3-FP. (c) CSE-4-FP.(d) PEO-LiTFSI.

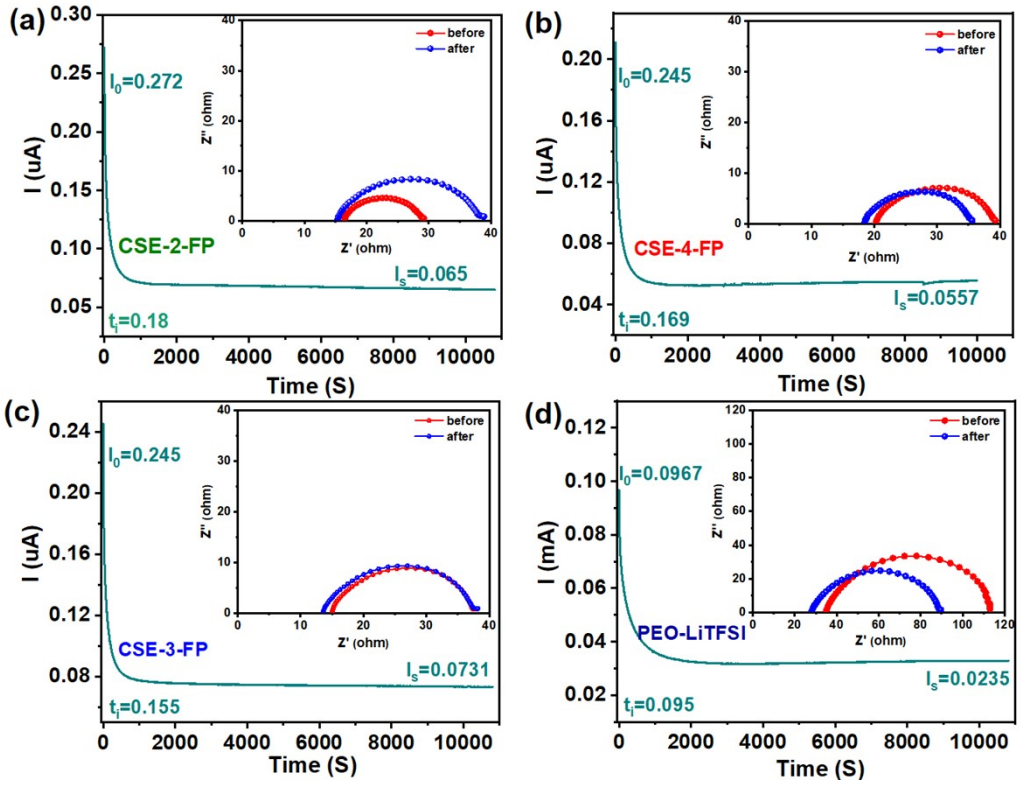

Figure S5. Chronoamperometric curve of the Li//CSE//Li cell after perturbation from 10 mV at 60 °C. (a) CSE-2-FP. (b) CSE-3-FP. (c) CSE-4-FP. (d) PEO-LiTFSI.

Table S2. Atomic ratios of the different elements in the SEI films formed in different electrolytes.

	C	N	F	O	Li
CSE-2-FP	21.45	0.28	6.83	46.13	25.31
CSE-3-FP	26.76	0.44	9.66	35.60	27.54
CSE-4-FP	23.96	0.32	6.32	43.86	25.54

Table S3. Ratios of C-F and LiF in different electrolytes

	C-F	LiF
CSE-2-FP	51	49
CSE-3-FP	15.7	84.3
CSE-4-FP	31	69

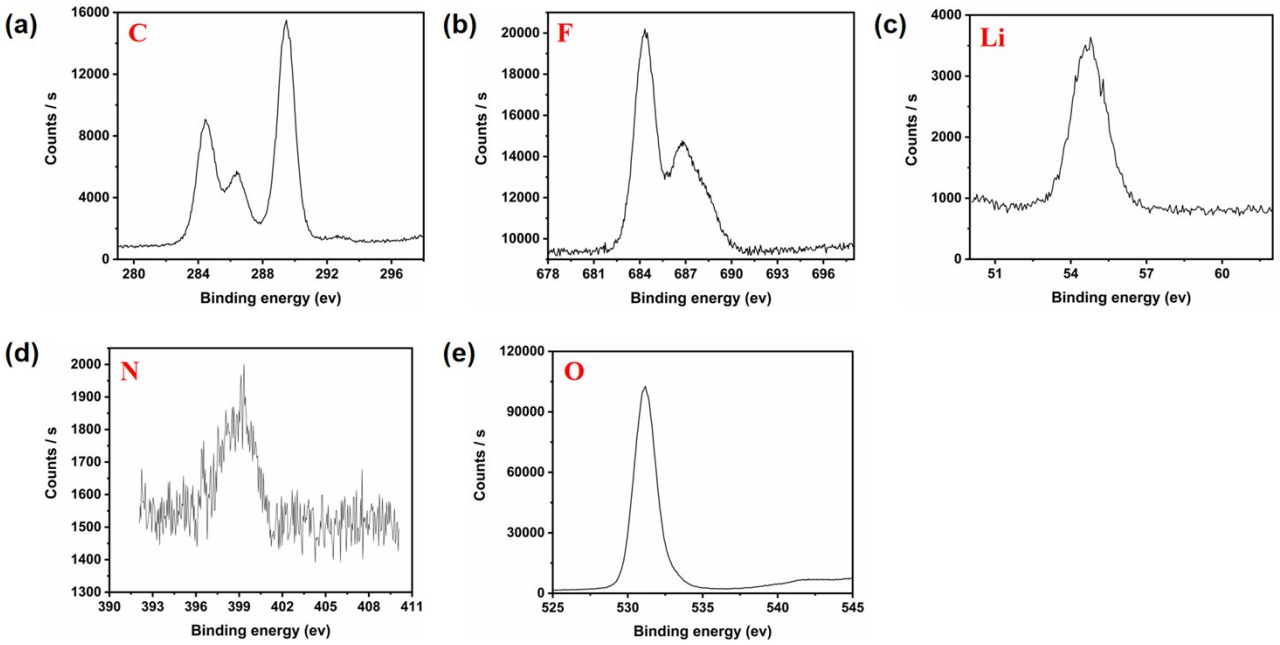

Figure S6. XPS survey scan of the lithium surface of CSE-2-FP

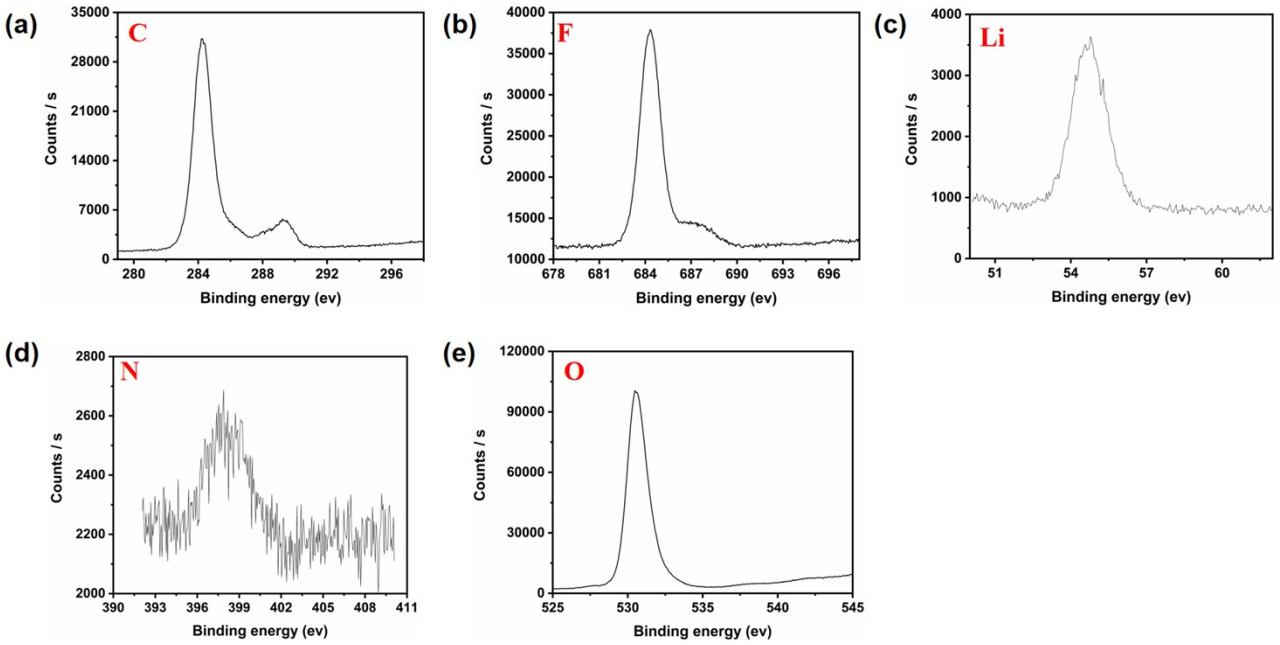

Figure S7. XPS survey scan of the lithium surface of CSE-3-FP

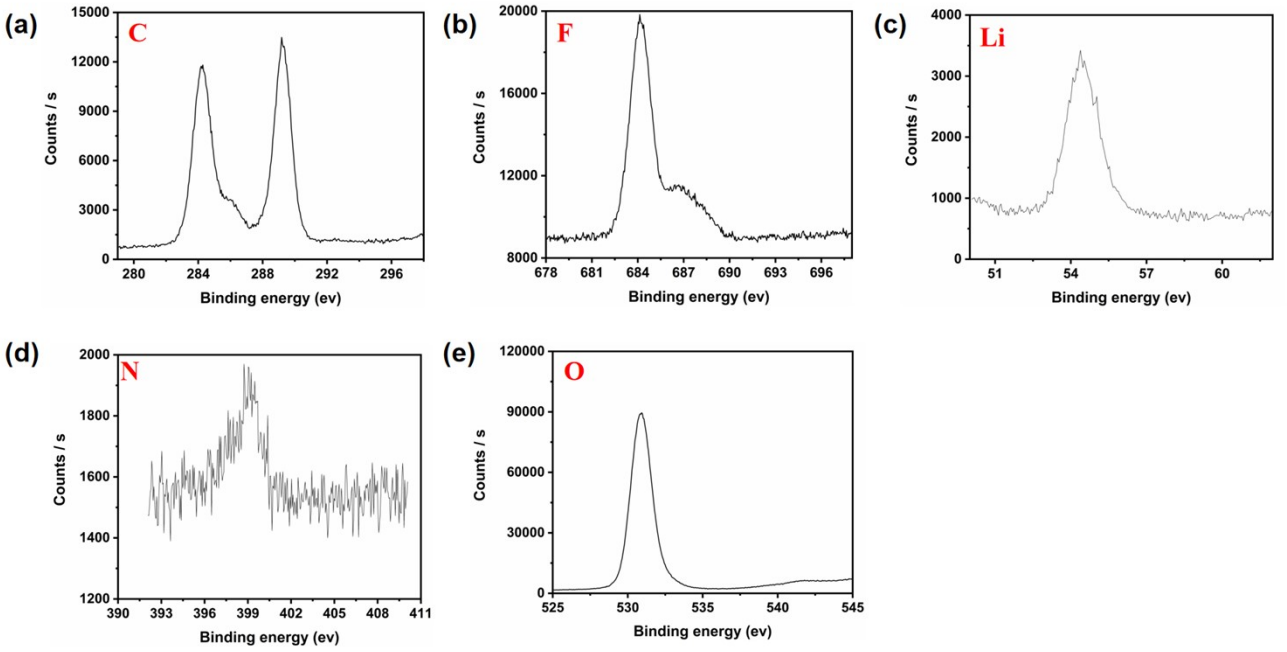

Figure S8. XPS survey scan of the lithium surface of CSE-4-FP

DFT calculation

We built the structures shown in Fig. 3d to investigate the effect of the F atom on the benzene ring in POPs-2-FP, POPs-3-FP, and POPs-4-FP on the C-F bond length in $TFSI^-$. The distance and orientation of the F atom in POPs-X-FP with respect to the C-F bond in TFSI- are the same, which eliminates the effect of distance and orientation. In all three structures, the valence electrons of the F atoms have been paired, indicating mutual repulsion between the F atoms and the C-F bonds, keeping them away from each other. Then, we performed structural relaxation using the first-principles package VASP based on density generalized theory. From the structure after relaxation, we can find that the C-F bond on the benzene ring of POPs-X-FP and the C-F bond of $TFSI^-$ are reduced, which is consistent with our analysis. Then, we provide the bond length changes before and after the relaxation, as shown in Table 1. We find that this result is consistent with the experimental observation that POPs-3-FP leads to the longest C-F bond in the $TFSI^-$, while POPs-4-FP having the second-longest C-F bond after POPs-3-FP, and POPs-2-FP having the weakest effect.

Table S4. The lengths of the C-F bond before and after relaxation of the $TFSI^-$ molecular structure in

the three structures, the unit is Å.

	C-F (POSCAR)	C-F (CONTCAR)
POPs-3-FP	1.35497	1.37722
POPs-4-FP	1.35498	1.37195
POPs-2-FP	1.35498	1.35945

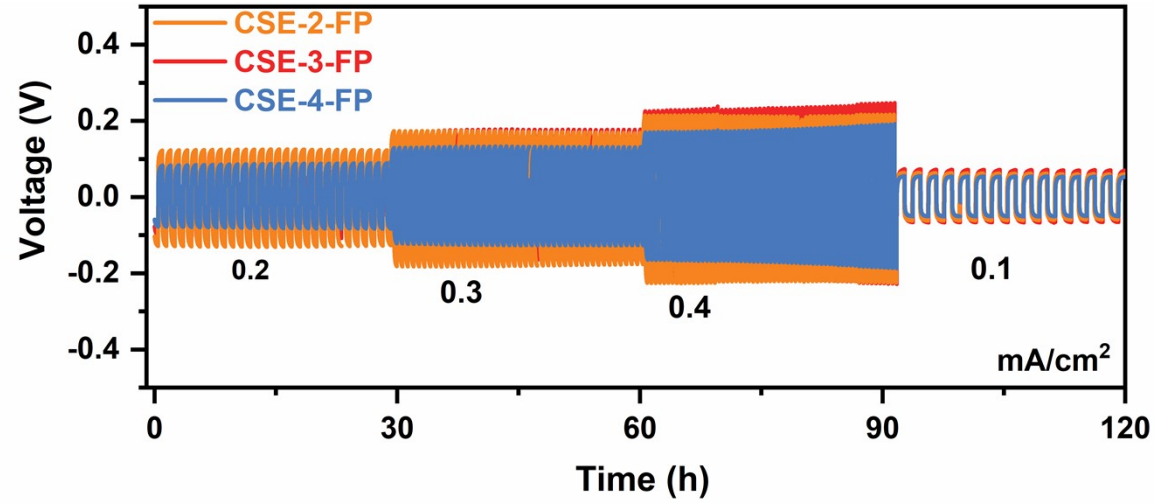

Figure S9. Galvanostatic cycling curves of the Li//CSE//Li cell at different current densities at 60 °C.

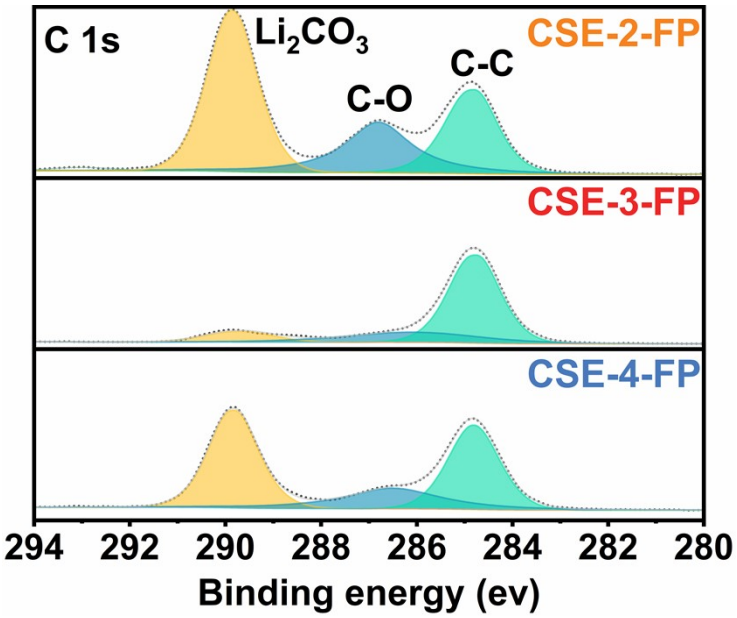

Figure S10. C 1 s XPS spectra of lithium surface from the Li//CSE//Li cell after cycling.

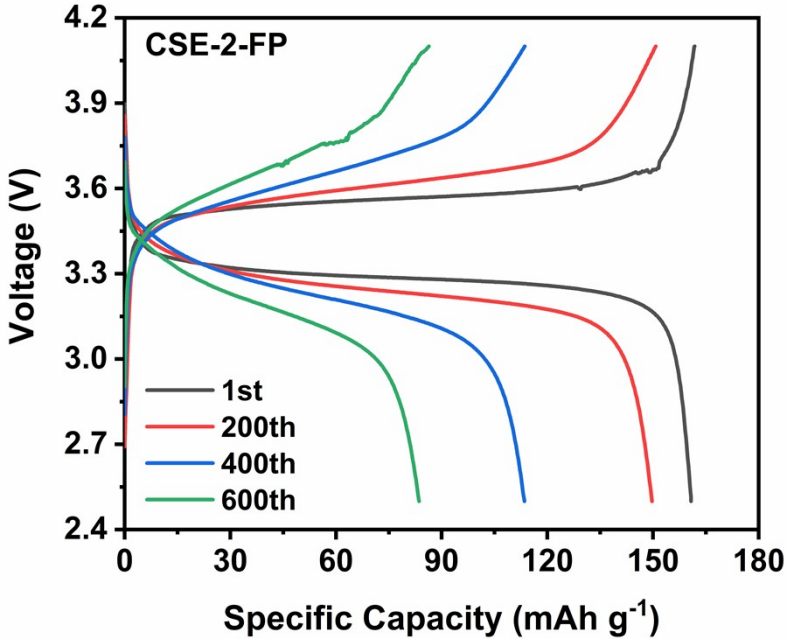

Figure S11. Voltage profiles of the LFP//CSE-2-FP//Li cell at 0.5C.

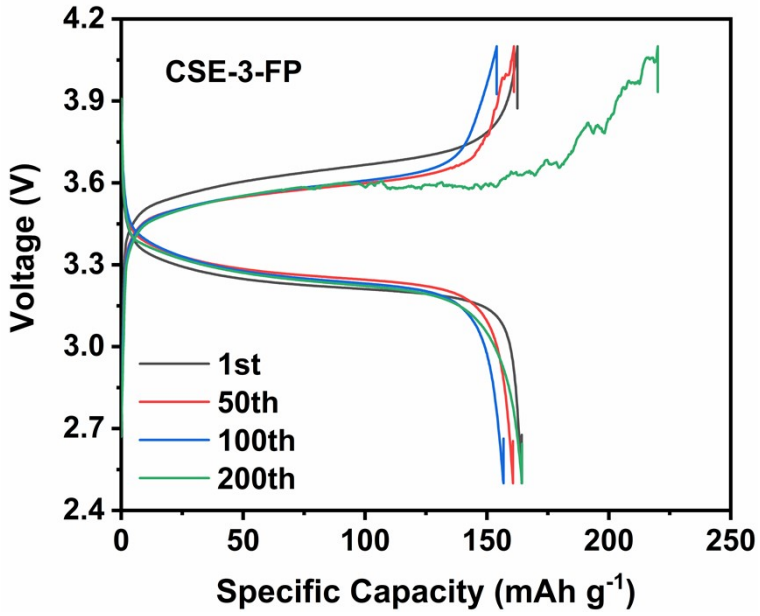

Figure S12. Voltage profiles of the LFP//CSE-3-FP//Li cell at 0.5C.

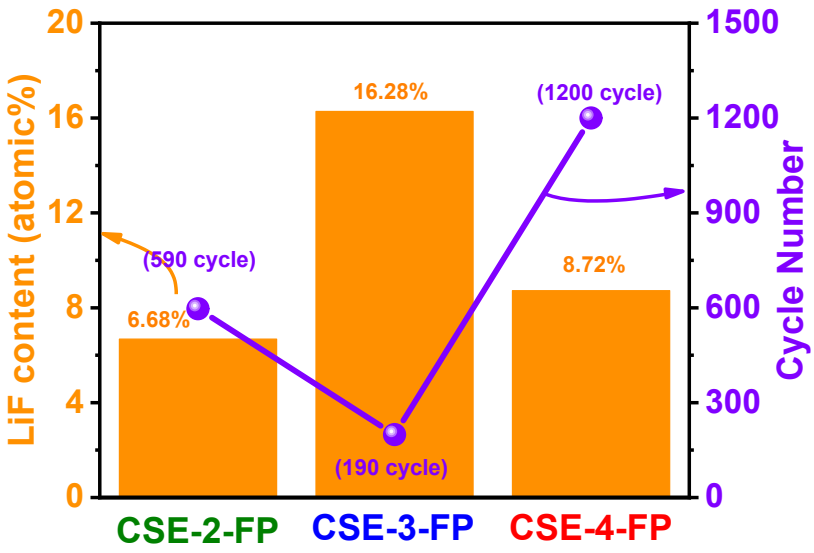

Figure S13. LiF content in different electrolytes and the corresponding cycle life of the LFP//CSE//Li cells.

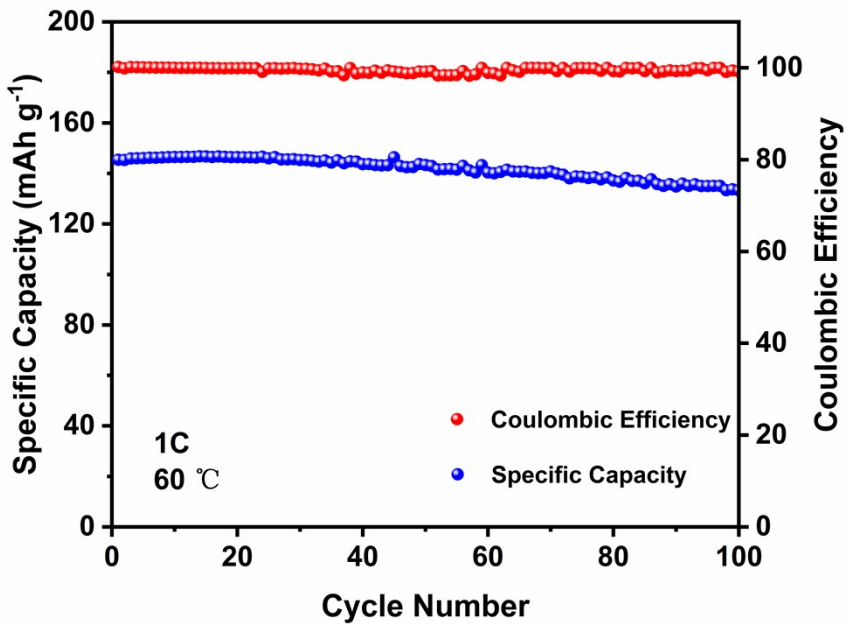

Figure S14. Cycling stability of the LFP//CSE-4-FP//Li cell at 1C.

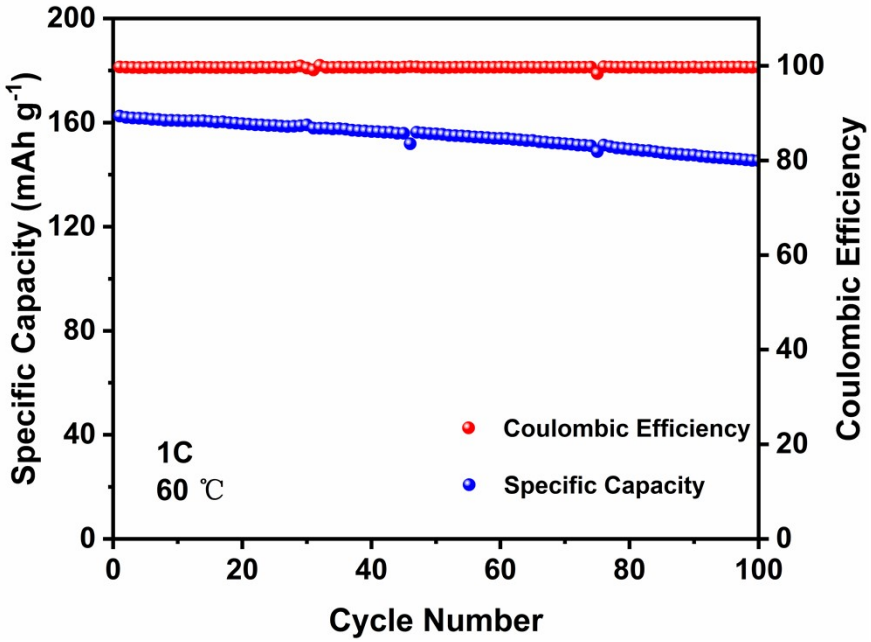

Figure S15. Cycling stability of the NCM811//CSE-4-FP//Li cell at 1C.

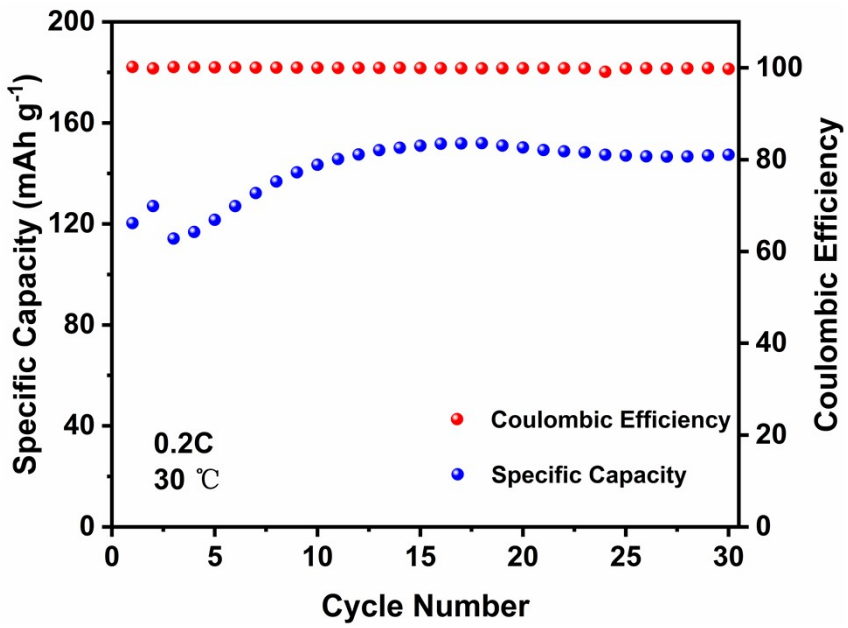

Figure S16. Cycling stability of the LFP//CSE-4-FP//Li cell at 0.2C.

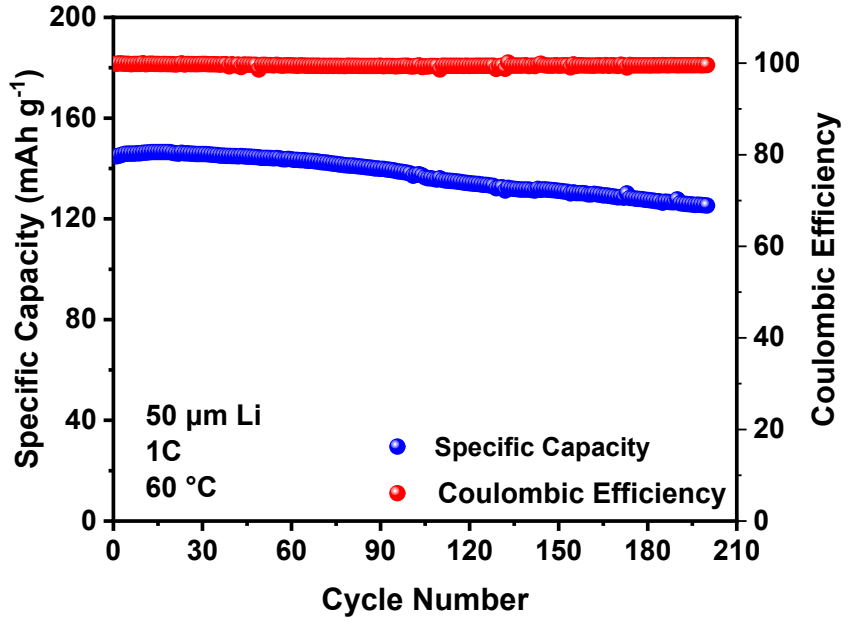

Figure S17. Cycling stability of the LFP//CSE-4-FP//thin-Li cell at 1C.